Available online at www.sciencedirect.com
ScienceDirect
Journal of Power Sources 171 (2007) 981–989
JOURNAL OF POWER SOURCES
www.elsevier.com/locate/jpowsour

Effects of surface coating of $Y(OH)_3$ on the electrochemical performance of spherical $Ni(OH)_2$

Jing Fan, Yifu Yang *, Peng Yu, Weihua Chen, Huixia Shao

College of Chemistry and Molecular Science, Wuhan University, Wuhan 430072, PR China

Received 5 February 2007; received in revised form 9 July 2007; accepted 12 July 2007
Available online 19 July 2007

Abstract

The effects of surface coating of $Y(OH)_3$ on the electrochemical performance of spherical $Ni(OH)_2$ were studied by cyclic voltammetry (CV) with soft-embedded electrode (SE-E). The coating was performed by chemical surface precipitation under different conditions. The structure, morphology, chemical composition and electrochemical properties of two different samples with surface coating of $Y(OH)_3$ were characterized and compared. The results show that a two-step oxidation process exists in the oxidation procedure of spherical $Ni(OH)_2$ corresponding to the formation of Ni(III) and Ni(IV), respectively. The conversion of Ni(III) to Ni(IV) is regarded as a side reaction in which Ni(IV) species is not stable. The presence of $Y(OH)_3$ on the particle surface can restrain the side reactions, especially the formation of Ni(IV). The application of coated $Ni(OH)_2$ to sealed Ni–MH batteries yielded a charge acceptance of about 88% at 60 °C. The results manifest that the high-temperature performance of $Ni(OH)_2$ electrode is related to the distribution of the adding elements in surface oxide layer of $Ni(OH)_2$, the sample with dense and porous coating surface, larger relative surface content and higher utilization ratio of yttrium is more effective.

Keywords: Spherical nickel hydroxide; Yttrium hydroxide; Soft-embedded electrode; Cyclic voltammetry; Ni(IV) species

1. Introduction

The properties of $Ni(OH)_2$ have been the subject of investigation for several decades due to its extensive application as the positive electrode material in secondary batteries [1–3]. However, a number of issues still exist concerning its electrochemical characteristics, particularly with regard to the oxidation state of the nickel in the charged electrode. The existence of Ni(IV) species has been suggested by many authors [4–12]. O'Grady et al. [4] gave out the first direct in situ evidence for the presence of Ni(IV) by utilizing X-ray absorption near edge structure (XANES) method to study the oxidation state of Ni in a fully charged nickel oxide electrode (NOE). The evidence for the existence of Ni(IV) was also supported by coulometry method [5,6], by the determination of trapped 'active oxygen' in the matrix by titration [7], and by ellipsometry measurements [8]. Previous studies also presented different functions of Ni(IV) species. On one hand, the formation of Ni(IV) could result in higher capacity [9,10], on the other hand, the mechanisms for oxygen evolution reaction could also be explained through the participation of Ni(IV) species [8,11]. Although there are numerous studies on Ni(IV) species, these results are still not complete. For example, it has been difficult to study the electrochemical properties of Ni(IV) species in spherical $Ni(OH)_2$ until now. Spherical $Ni(OH)_2$ is the currently prevailing form of $Ni(OH)_2$ for battery manufacturing [3]. Therefore, it is of both academic and technical significance to obtain detailed information about Ni(IV) species in spherical $Ni(OH)_2$. In this paper, a two-step oxidation process of spherical $Ni(OH)_2$ was observed by using a soft-embedded electrode (SE-E). This method does not use any additives that function as binder or electric conductor, so the influence from these additives can be avoided. The presence and the stability of Ni(IV) species were further discussed.

To improve the performance of $Ni(OH)_2$ electrode, especially in Ni/MH batteries, yttrium additives have been widely used and showed comprehensive features. The addition of Y_2O_3 increased $Ni(OH)_2$ utilization [13]. The doping of yttrium could significantly improve the performance of $Ni(OH)_2$ at elevated temperature, such as the charge acceptance could be raised up from 41 to 82% at 60 °C [14]. The $Y(OH)_3$-coated $Ni(OH)_2$

* Corresponding author. Tel.: +86 27 87218624; fax: +86 27 68754067.
E-mail address: yang-y-f1@vip.sina.com (Y. Yang).

0378-7753/$ – see front matter © 2007 Elsevier B.V. All rights reserved.
doi:10.1016/j.jpowsour.2007.07.030

tube electrode also exhibited excellent charge/discharge performance, especially at high-rate and high-temperature [15]. However, previous researchers focused their major attentions to the effects of yttrium additives on oxygen evolution and Ni(II) oxidation reactions, but paid much less attentions to its effect on Ni(IV) species. In this study, the side reaction corresponding to the formation of Ni(IV) is observed and proved to be suppressed by $Y(OH)_3$ coating on $Ni(OH)_2$ surface. The effects of two coated samples with diverse morphologies were compared. And then, the comprehensive performances of yttrium additives were interpreted reasonably in detail.

2. Experimental

2.1. Preparation and characterization of spherical $Ni(OH)_2$ coated with $Y(OH)_3$

The spherical $Ni(OH)_2$ particles (sample A) with diameter of about 8–12 μm were obtained by separating them from a commercial available β-$Ni(OH)_2$ product. $Y(OH)_3$ coating on spherical $Ni(OH)_2$ particles was performed in the following way: a certain amount of sample A was added into a container with distilled water under agitation to form suspension solution. Subsequently, YCl_3 solution was dropped stepwise into the suspension solution under magnetic stirring at 50 °C, during the process the pH value of the reaction solution was controlled between 6.5 and 8.5. Finally, the product was washed with ultrapure water, filtered and dried at 65 °C. For comparison reason, two samples (i.e. B and C) were prepared by changing the concentration of YCl_3 solution and pH value, the preparation conditions are listed in Table 1. Depending on the preparative conditions the surface morphology of $Ni(OH)_2$ particles was changed greatly.

Crystal phase structure of the samples was analyzed by powder X-ray diffraction (XRD-6000, Shimadzu, Japan) with Cu Kα radiation. Surface images were characterized with a scanning electron microscope (SEM, Hitachi X-650, Japan). The surface condition of the samples was tested by an X-ray photoelectron spectrum (XPS, XSAM800, Kratos). A quantitative measurement of the ratio of yttrium to nickel was obtained by dissolving the samples in 1.2 mol L^{-1} HCl and by analyzing the solutions with Inductively Coupled Plasma (ICP) spectrometry (Intrepid XSP Rasial, Thermo, USA).

2.2. Preparation of nickel electrodes

The structure of soft-embedded electrode (SE-E) is schematically shown in Fig. 1. SE-E was prepared in following way.

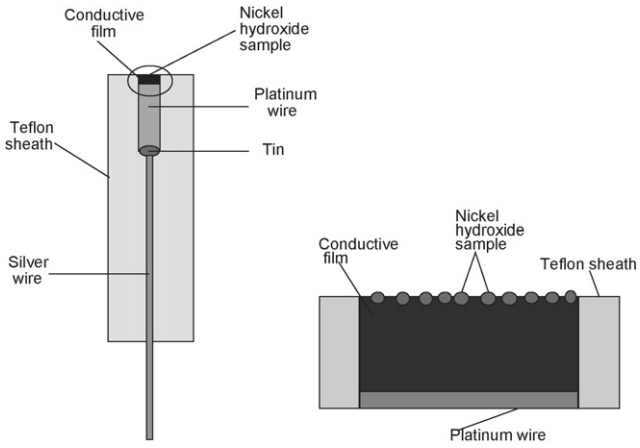

Fig. 1. Block scheme of soft-embedded electrode (SE-E).

Firstly, a 2 mm diameter platinum disc with a conducting wire was sealed into a Teflon holder. Secondly, a PTFE bonded acetylene black membrane was impregnated in melting microcrystalline wax (melting point: 352 K), removed and cooled. A piece of the membrane was cut out with a special knife, so that the membrane had the same diameter as that of disk electrode hole. Thirdly, this piece of membrane was pressed into disk hole, and then polished. Finally, a small amount of the test sample was carefully and uniformly embedded on the surface of the membrane.

The pasted $Ni(OH)_2$ electrodes were prepared as follows: 88 wt.% sample, 7 wt.% CoO and 5 wt.% Ni powder were thoroughly mixed with 2 wt.% PTFE solution to form a slurry. Then the slurry was pasted into nickel foam to form a 2 cm × 2 cm electrode. After drying at 65 °C for 1 h, the pasted $Ni(OH)_2$ electrode was pressed at a pressure of 30 MPa for 1 min.

2.3. Electrochemical measurements

CV measurements were carried out in a classical three-electrode cell with an electrochemistry workstation (CHI660B, Chenhua instrument Ltd., Shanghai). A SE-E embedded with the test sample was used as working electrode, the counter electrode was a Pt foil, and the reference electrode was a home made Hg/HgO immersed in 6 mol L^{-1} KOH electrolyte prepared with KOH (G.R) and ultrapure water (resistivity ≥18 MΩ, water purification system). The reference electrode was connected to the cell by a luggin capillary. All potentials shown in CV measurements were measured against this reference electrode. A 6 mol L^{-1} KOH solution was applied as the electrolyte. The test temperatures ranged from 25 to 55 °C.

Table 1
Precipitation conditions and relative element content for different samples

Sample	PH value of the reaction solution	Yttrium concentration (mmol L^{-1})	Molar ratio on the surface[a]	Molar ratio in total[b]
			Y:Ni	Y:Ni(%)
B	6.5–7.5	5	2.19	0.55
C	7.5–8.5	20	7.77	0.55

[a] Molar ratio (%) of Y to Ni as determined by XPS.
[b] Molar ratio (%) of Y to Ni as determined by ICP.

Charge/discharge studies were conducted with a Battery Testing Equipment (Land Test Equipment, CT2001A) in a sealed test cell, including the pasted nickel electrode as the cathode, a commercial hydrogen-storage alloy electrode as the anode and a 6 mol L^{-1} KOH solution as the electrolyte, the anode and cathode were separated by a commercial available separator. Before test, the cells were charged and discharged at 0.2*C* rate for several times for activation. The charge acceptance of the test cell was measured at 1*C* rate with about 10% overcharge and a cut-off voltage of 1.0 V for discharge at 25 and 60 °C.

3. Results and discussion

3.1. Cyclic voltammograms (CVs) recorded with SE-E

The CVs measured with a blank SE-E in 6 mol L^{-1} KOH solution at a scan rate of 2 mV s^{-1} are shown in Fig. 2. The curves recorded from cycle 1 to cycle 500 at 25 °C have a little change, indicating that no significant structure and surface change takes place on the blank SE-E during the scan. The reproduced curves could be attained, after the electrode surface was soaked in 6 mol L^{-1} KOH for three days. These results indicate that the SE-E had the long cycle life and high stability in 6 mol L^{-1} KOH solution. The current response ranges from 0.1 nA to 1.5 μA in the potential window of 0–0.65 V at 25 °C and 55 °C.It is negligible as compared with those of the $Ni(OH)_2$ samples as shown later.

The CVs of the SE-E embedded with spherical $Ni(OH)_2$ particles at various scan rate after activation are shown in Fig. 3. One important feature on the CVs of Fig. 3 is that there are two distinct oxidation current peaks (O1 and O2), and only one reduction current peak (R1), respectively. The potential of peak O2 (E_{O2}) appears prior to that of oxygen evolution (E_{OE}), but is at more positive value than that of peak O1 (E_{O1}). The difference between E_{O1} and E_{O2} is about 95 mV. Similar features were observed in the analogous measurements of at least 20 different

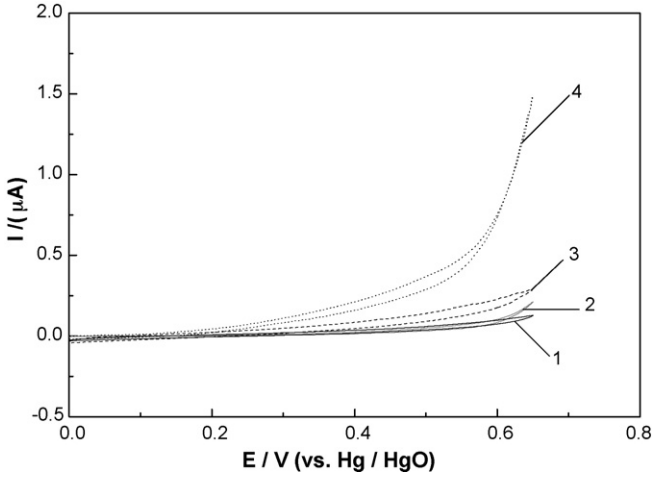

Fig. 2. Cyclic voltammograms of blank SE-E in 6 mol L^{-1} KOH solution. Potential range: 0–0.65 V; scan rate: 2 mV s^{-1}; (1) first cycle at 25 °C; (2) after soaking for 3 days; (3) 500th cycle at 25 °C; (4) first cycle at 55 °C.

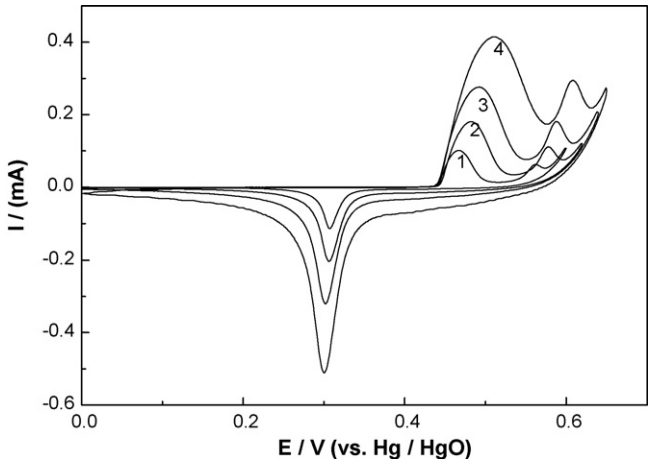

Fig. 3. Cyclic voltammograms of spherical $Ni(OH)_2$ at 25 °C and various scan rates: (1) 0.2 mV s^{-1}, (2) 0.5 mV s^{-1}, (3) 1 mV s^{-1} and (4) 2 mV s^{-1}; potential range: (1) 0–0.6 V, (2) 0–0.62 V, (3) 0–0.64 V and (4) 0–0.65 V.

spherical $Ni(OH)_2$ samples with diverse contents, indicating that the appearance of these two oxidation peaks was not caused by certain extrinsic effects e.g. additives, but related to the intrinsic characteristics of spherical $Ni(OH)_2$.

Different interpretations to these two oxidation peaks could be found in literatures [9,10,18–20], most of which were related to phase change or the formation of higher oxidation states. As the possibility of phase change in the charging process is taken for consideration, it is well known that trivalent β-NiOOH can be transformed into γ phase upon overcharge and high electrolyte concentrations [16]. Moreover, γ-NiOOH can be reduced to α-$Ni(OH)_2$, which is unstable and most of it can be transformed to β-$Ni(OH)_2$ during the reverse scan [17]. Accordingly, the oxidation peaks were supposed to be the transformation of β-$Ni(OH)_2$ to β-NiOOH (O1) and α-$Ni(OH)_2$ to γ-NiOOH (O2), respectively. However, the potential of α-$Ni(OH)_2$/γ-NiOOH reaction is generally 20 to 50 mV lower than the value of β-$Ni(OH)_2$/β-NiOOH reaction [9,18–20], whereas the present work shows a higher peak potential of the second oxidation peak and a peak separation of about 95 mV which is larger than the supposed value. So the possibility of the reaction of α-$Ni(OH)_2$/γ-NiOOH for wave O2 is unreasonable.

Another interpretation to these two oxidation peaks is the successive transitions of $Ni(OH)_2$: Ni(II) → Ni(III) (O1) and Ni(III) → Ni(IV) (O2). It is generally accepted that Ni(IV) species is formed on overcharge [4–6,21], or in the process of oxygen evolution [8,11]. Moreover, the peak separations between different oxidation states (Ni(III) and Ni(IV)) are usually more than 90 mV [10,22]. With the data shown in Fig. 3, wave O2 is overlapped with oxygen evolution reaction, and this case becomes more serious at lower scan rate. These results strengthen the designation of the peaks to various oxidation states rather than to different phases. Thus, these two oxidation peaks can be explained as the transformation of Ni(II) to Ni(III) and Ni(III) to Ni(IV).

In addition, the electric charge of cathodic peak ranges from 23.3 mQ and 24.7 mQ for the scan rates investigated, this indicates that the majority of embedded particles have been involved

in the reaction. Thus, the potential scan rate was set as 2 mV s^{-1} in the following CV measurements.

It should be mentioned that the unique features observed in this study is owed to the better performance of SE-E. In this case, $Ni(OH)_2$ particles can be well distributed on the electrode surface, adequately contacted by electrolyte for a majority of particles and strongly fixed by conductive membrane without any other additives, e.g. binder. While on traditional pasted $Ni(OH)_2$ electrodes [3,15,23] the two-step oxidation process of spherical $Ni(OH)_2$ is difficult to observe due to the affects of additives and the complicated porous structure of the electrode.

3.2. Electrochemical properties of Ni(IV)

As the presence of Ni(IV) has been verified above, the stability of Ni(IV) species becomes a more important issue. To get a better understanding of this, CVs were measured over a wide range of potential windows including: 0–0.60, 0–0.62, 0–0.64 and 0–0.66 V at 25 °C, and 0–0.57, 0–0.60 and 0–0.63 V at 45 °C, the results are shown in Fig. 4(a) and (b). The features of the voltammograms are summarized in Table 2. The XPS analysis was performed after the potential reached 0.64 V without return sweep. It is understandable that if Ni(IV) species is stable enough that it can be electrochemically reduced in the cathodic process, it can lead to a marked increase in electrode capacity [10,24,25]. However one can see from Fig. 4 and Table 2 that, though the total electric charge of the anodic process (Q_{ox}) increased due to Ni(IV) formation and oxygen evolution as the upper potential limit of CV was set at more positive values at 25 °C, the electric charge of cathodic peak (Q_{red}) was practically kept constant, no significant contribution from the reduction of Ni(IV) was observed. And meanwhile, as shown in Fig. 5, there is no evidence for the appearance of Ni(IV) species in XPS results. Similar XPS results could also be found in literatures studying the charge process of spherical β-$Ni(OH)_2$ [26]. These results clearly indicate the instability of Ni(IV) species in spherical β-$Ni(OH)_2$. The slight increase in Q_{red} can be accounted for more complete conversion of Ni(II) to Ni(III) at higher potential, but this contribution is too small to affect the height and size of wave O2 after the upper potential exceeds 0.6 V. Similar features were also observed at 45 °C, but the proportion of Q_{red} became smaller due to the enhanced influence of Ni(IV) formation and oxygen evolution reactions.

In general, the conversion of Ni(III) to Ni(IV) can be supposed to take place in the bulk as well as on the surface layer of spherical $Ni(OH)_2$ particle, which can lead to distinct functions of Ni(IV) species. Some researchers [8,11,27] reported that

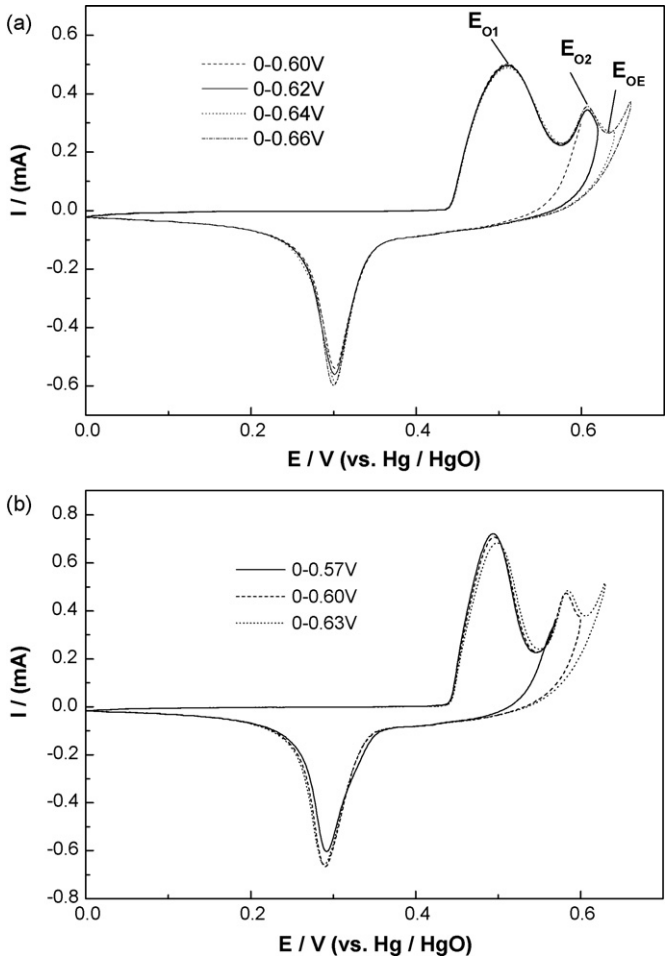

Fig. 4. Cyclic voltammograms of spherical $Ni(OH)_2$ in different potential range: (a) 0–0.60, 0–0.62, 0–0.64 and 0–0.66 V at 25 °C; (b) 0–0.57, 0–0.60 and 0–0.63 V at 45 °C. Scan rate: 2 mV s^{-1}.

the surface oxide layer of the nickel active material offered the most favorable site for oxygen evolution reaction. Thereinto, Ni(IV) species such as NiO_2 could act as such an intermediate, and it could dissociated into Ni(III) species and oxygen. Whereas others [10,24] found that when large amounts of cobalt were present, nearly all the Ni(II) could be oxidized into Ni(IV) and almost all the oxidized active material could be reduced to Ni(II). In such a case, the presence of considerable amounts of Ni(IV) species led to a marked increase in electrode capacity. As described vide ante, it is reasonable to consider that the conversion of Ni(III) to Ni(IV) takes place on the surface layer of spherical $Ni(OH)_2$ particles. In this case, Ni(IV) species is not stable and may totally convert to Ni(III) species soon after its

Table 2
Integrated charges in nickel hydroxide redox couple

Charge (mC)	Potential windows (25 °C)				Potential windows (45 °C)		
	0–0.60 V	0–0.62 V	0–0.64 V	0–0.66 V	0–0.57 V	0–0.60 V	0–0.63 V
Q_{ox}	26.0	29.0	32.0	35.0	26.5	32.3	38.4
Q_{red}	22.1	22.4	22.5	22.6	24.0	25.4	25.5
Q_{red}/Q_{ox}	0.85	0.77	0.70	0.65	0.91	0.79	0.66

Q_{ox}: total anodic charge; Q_{red}: charge of cathodic peak.

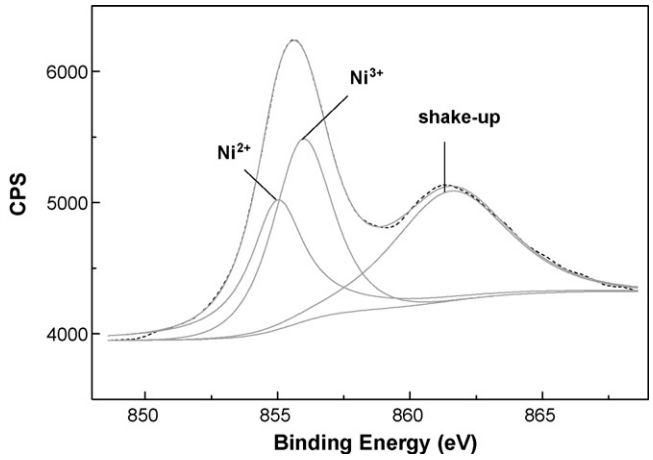

Fig. 5. XPS spectrum of Ni2$p_{3/2}$ region. Dash line: original curve recorded by XPS; solid line: fitted line.

formation. On the other hand, the appearance of the wave O2 in our CV tests provide the convictive evidence for the presence of higher unstable oxide in spherical β-Ni(OH)$_2$ which is generally considered as a possible intermediate of oxygen evolution reaction [8,28]. However, due to the instability of Ni(IV) species, other direct evidences for the presence of Ni(IV) species in spherical β-Ni(OH)$_2$ are still unavailable at present.

Above results manifest that the transition of Ni(III) to Ni(IV) is a side reaction which functions as to reduce the charge efficiency of Ni(OH)$_2$ material. From Fig. 4 it is obvious that the potential range of the oxidation reactions of Ni(II) and Ni(III) are overlapped seriously. As the temperature is raised up, the difference between E_{O1} and E_{O2} becomes smaller (see Fig. 4 (b)), and meanwhile the size and height of current peak O2 increase. As a result, the potential range overlap of the two reactions becomes more serious. Therefore, at elevated temperatures the charge acceptance decreases not only owing to the direct oxygen evolution reaction, but also relating to the oxidation reaction of Ni(III) which could result in an indirect oxygen evolution [8]. So it is necessary to restrain the formation of Ni(IV).

3.3. Characterization of spherical Ni(OH)$_2$ coated with Y(OH)$_3$

To restrict the influence of side reactions on the charge efficiency of Ni(OH)$_2$, many efforts have been evaluated in the past, in which the addition of Y element seems to be one of the most effective way[13–15]. Mi et al. [14] reported that the enriched yttrium on the surface of Ni(OH)$_2$ was beneficial to controlling the oxygen evolution of Ni(OH)$_2$ electrode. However, the chemical nature and morphology of the yttrium-rich surface and corresponding effects on side reactions are still unknown. For that reason, samples B and C with different coating surface were prepared. Fig. 6 shows X-ray diffraction patterns of the three samples in which the samples B and C were processed with surface coating of Y(OH)$_3$. The result indicates that there is no difference in the diffraction patterns between uncoated and coated Ni(OH)$_2$, probably it is because the coating amount of Y(OH)$_3$ is too small to be detected by XRD analysis. For

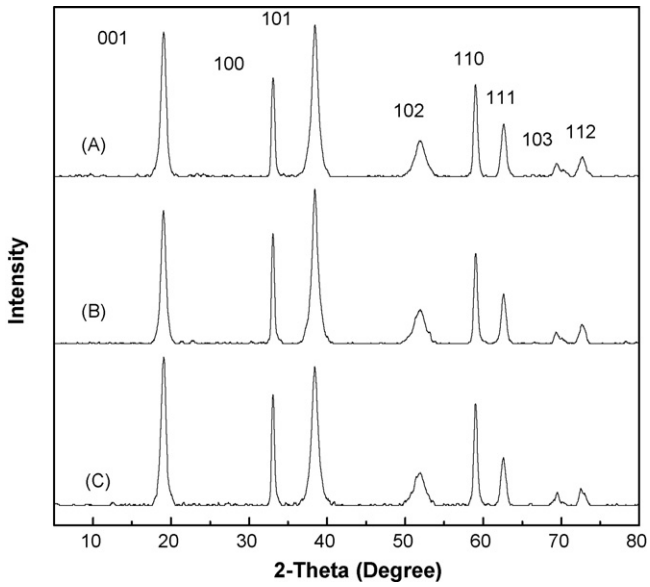

Fig. 6. XRD patterns of samples A–C: (A) sample A; (B) sample B; (C) sample C.

comparison reason, the X-ray diffraction pattern of the Y(OH)$_3$ precipitate prepared under the same condition of the preparation process of sample C with the absence of Ni(OH)$_2$ was also detected and the data is given in Fig. 7. It is found that the yttrium hydroxide presents very low crystallinity.

The SEM images of the samples are illustrated in Fig. 8. At relatively low magnification (2500×), the Ni(OH)$_2$ particles with surface coating of Y(OH)$_3$ (samples B and C) maintain the same shape and size as that of the precursor Ni(OH)$_2$ (sample A). However at high magnification (40,000×), the uncoated Ni(OH)$_2$ particles (sample A) show a smooth and porous surface which is made up of stacks of needle-like and flake-like Ni(OH)$_2$ tiny crystals, and the morphology of coated Ni(OH)$_2$ particles (samples B and C) depend strongly on the experimental conditions of the surface coating as described in Table 1. The condition of relatively high solution pH value (7.5–8.5) and yttrium concentration (20 mmol L^{-1}) resulted in a particle-like coating with coarse surface (sample C), whereas the condition of relatively low solution pH value (6.5–7.5) and yttrium concen-

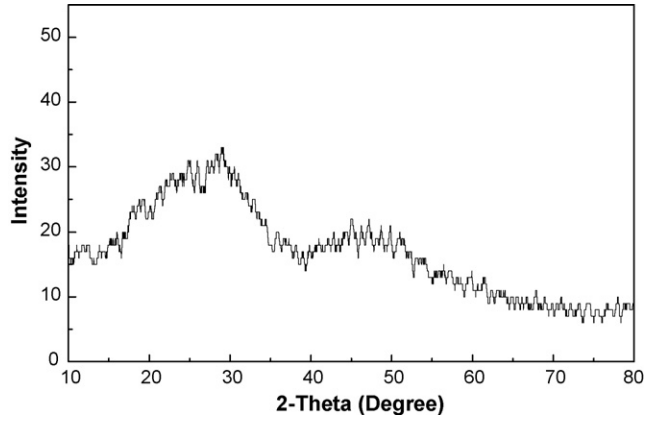

Fig. 7. XRD pattern of Y(OH)$_3$ precipitate prepared under the same condition of the preparation process of sample C with the absence of Ni(OH)$_2$.

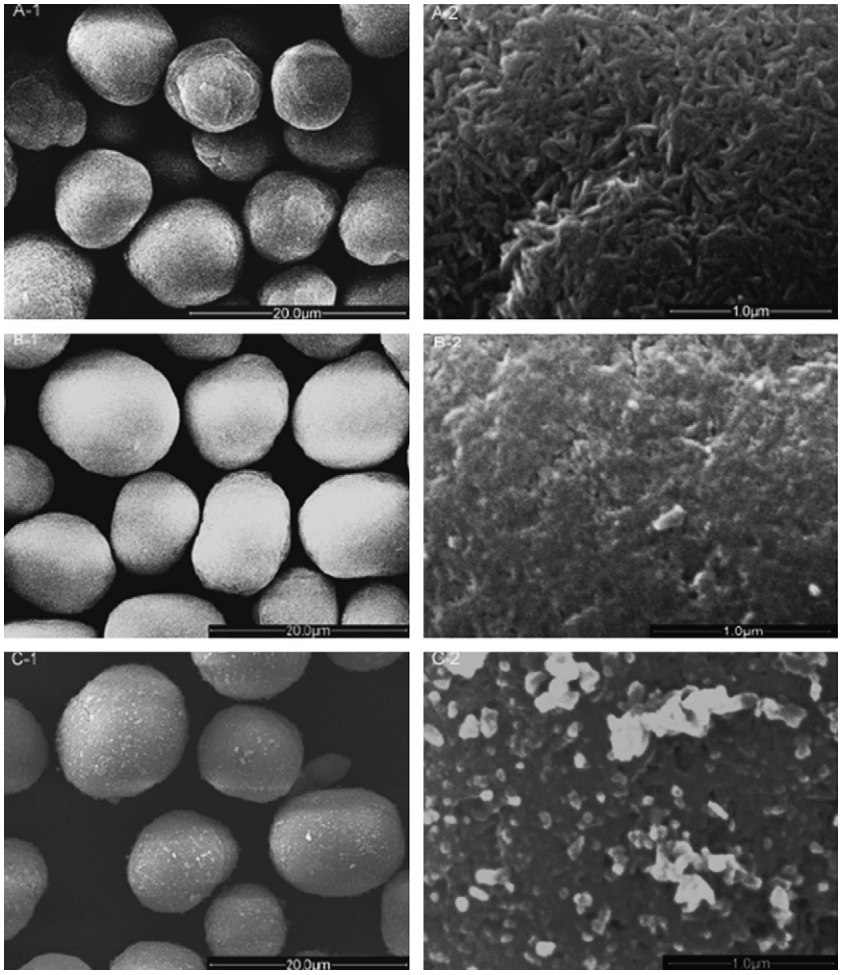

Fig. 8. SEM images of samples A–C. (A-1 and A-2) Sample A; (B-1 and B-2) sample B; (C-1 and C-2) sample C.

tration (5 mmol L^{-1}) yielded a continuous coating with smooth and dense surface (sample B).

From Table 1, it can also be seen that the molar ratio of element Y to Ni for both samples B and C is 0.55% obtained by ICP analysis, while the XPS results show that the molar ratio of Y:Ni on the surface of the samples B and C is 2.19 and 7.77, respectively. Therefore it is no doubt that the coating element is enriched in the surface layer of the particles.

3.4. CV measurements of spherical $Ni(OH)_2$ coated with $Y(OH)_3$

CVs of the SE-E embedded with samples A, B and C, respectively are shown in Fig. 9. The main features of the voltammograms are listed in Table 3 in detail. It can be seen from Table 3 that, firstly, by coating the spherical $Ni(OH)_2$ particles surface with $Y(OH)_3$, the oxidation potential of Ni(II) and Ni(III) shift to the less and more positive value, respectively. As a result the difference between E_{O2} and E_{O1} becomes larger. Except this, the peak potential separation between E_{O1} and E_{R1}, which can be considered as a measure of the reversibility of the electrode reaction (Ni(II) → Ni(III)) becomes smaller. These results elucidate that the presence of $Y(OH)_3$ coating makes the formation of Ni(IV) a more difficult process and favors the transition of Ni(II) to Ni(III) to be more easy and more reversible. Secondly, the potential difference between the oxygen evolution and the oxidation of Ni(II) becomes larger. Similar result was attained on the electrode containing $Y(OH)_3$-coated $Ni(OH)_2$ tube [15].

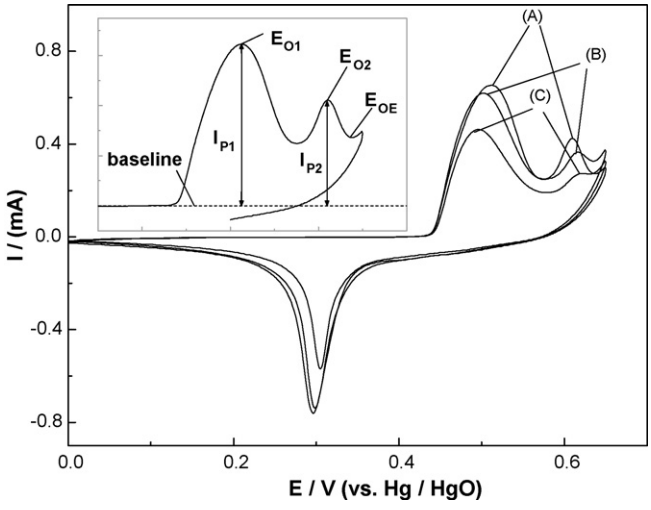

Fig. 9. Cyclic voltammograms of three samples in 6 mol L^{-1} KOH solution at 25 °C. Scan rate: 2 mV s^{-1}; potential range: 0–0.65 V. (A) Sample A; (B) sample B; (C) sample C.

Table 3
Potential values of CV features for different samples

Sample	Potential (V)						
	E_{O1}	E_{O2}	E_R	E_{OE}	$E_{O1}-E_R$	$E_{O2}-E_{O1}$	$E_{OE}-E_{O1}$
A	0.512	0.609	0.296	0.637	0.216	0.097	0.125
B	0.503	0.617	0.298	0.635	0.205	0.114	0.132
C	0.496	0.621	0.305	0.631	0.191	0.125	0.135

E_{O1}: oxidation potential of Ni(II); E_{O2}: oxidation potential of Ni(III); E_R: reduction potential; E_{OE}: oxygen evolution potential.

Further insight into the intensity of oxidation current peaks, there are two distinct anodic peak currents: I_{p1} and I_{p2} as plotted in Fig. 9. In cyclic voltammograms, anodic peak current represents the maximum of the electron transference in unit time in the charging process. I_{p1} is deemed as the maximum electron transference rate of main reaction (Ni(II) oxidation reaction). The significance of I_{p2} appears more complex than that of I_{p1}. The potential ranges for oxygen evolution and Ni(III) oxidation lie close to one another, so I_{p2} represents a combination of fluxes contributed by both Ni(III) oxidation and oxygen evolution reactions. I_{p2} is also influenced by the Ni(II) oxidation reaction, but it is in a negligible degree as shown in Section 3.2. Thus, I_{p2} represents the maximum electron transference rate of side reactions (including both the Ni(III) oxidation and the oxygen evolution reactions) in the potential range of Ni(IV) formation. It is obvious that the smaller the intensity of I_{p2} is, the more fully the electrode can be charged. For spherical $Ni(OH)_2$, both the oxygen evolution and the Ni(III) oxidation reactions are surface dependent, and the real superficial area has a strong correlation to the sample amounts, so it is difficult to compare the intensities of I_{p2} of the different samples directly. Thus, for sample A, I_{p2} with various intensities were plotted against the relevant I_{p1}, the result is shown in Fig. 10. For comparison purpose, the intensities of I_{p2} against the relevant I_{p1} for samples B and C were also recorded and drawn in Fig. 10. It is easy to notice that after $Y(OH)_3$ coating, the intensity of I_{p2} is significantly lowered as compared with the result of sample A at the same I_{p1} value. In other words, in the potential range close to main reaction the

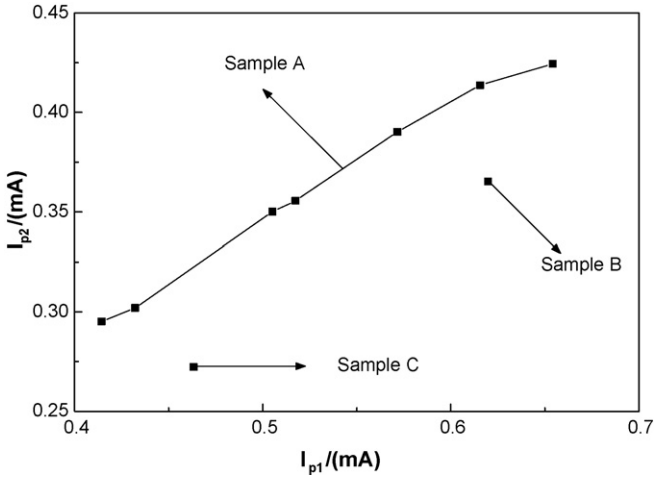

Fig. 10. I_{p2} vs. I_{p1} for three samples.

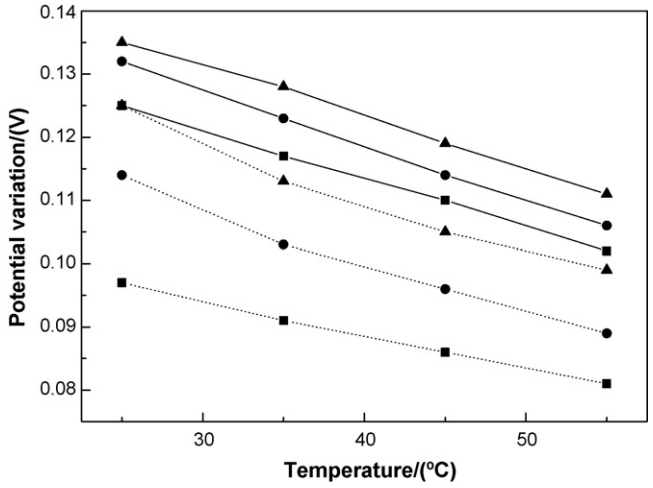

Fig. 11. Variation of $E_{O2}-E_{O1}$ and $E_{OE}-E_{O1}$ with temperature. Solid line: $E_{OE}-E_{O1}$ vs. T; dotted line: $E_{O2}-E_{O1}$ vs. T. (■) sample A; (●) sample B; (▲) sample C.

electron transference rate of side reactions can be restricted by surface coating of $Y(OH)_3$.

To further investigate the effect of $Y(OH)_3$ coating, CVs for samples A, B and C were measured at elevated temperatures, the variation of $E_{O2}-E_{O1}$ and $E_{OE}-E_{O1}$ with temperature are drawn in Fig. 11. Clearly, $Y(OH)_3$ coating on $Ni(OH)_2$ surface enlarges the potential difference between the main and the side reactions at elevated temperatures, especially between the oxidation reactions of Ni(II) and Ni(III). From Fig. 11, it is also clear that the effects of $Y(OH)_3$ coating are diverse for different samples. Sample C is more effective than sample B, although the additive amounts of these two samples are nearly the same. The difference may be caused by the diverse morphologies and chemical nature for different samples, and this will be discussed later.

From the above discussion, it can be concluded that the coating layer of $Y(OH)_3$ can effectively restrain the side reactions, especially the formation of Ni(IV). However, since the surface of spherical $Ni(OH)_2$ cannot be covered with $Y(OH)_3$ absolutely, we can still observe two oxidation peaks after $Y(OH)_3$ coating. Additionally, it is obvious that the chemical nature and morphology of the coating layer also play an important role in controlling the oxygen evolution and the Ni(III) oxidation reactions, which were reported fewer before.

3.5. Charge/discharge behavior of spherical $Ni(OH)_2$ coated with $Y(OH)_3$

In practical application, altering the surface condition of the spherical $Ni(OH)_2$ will generally bring on the corresponding change of the performance of Ni/MH cells, such as specific discharge capacity, charge acceptance, etc. [29–32]. To evaluate the practical effects of $Y(OH)_3$ coating and find possible control parameters to the high-temperature performance of $Ni(OH)_2$ electrode, the charge/discharge tests were performed. The charge/discharge curves of samples A, B and C at 1C rate and 25 °C measured by pasted type electrode are shown

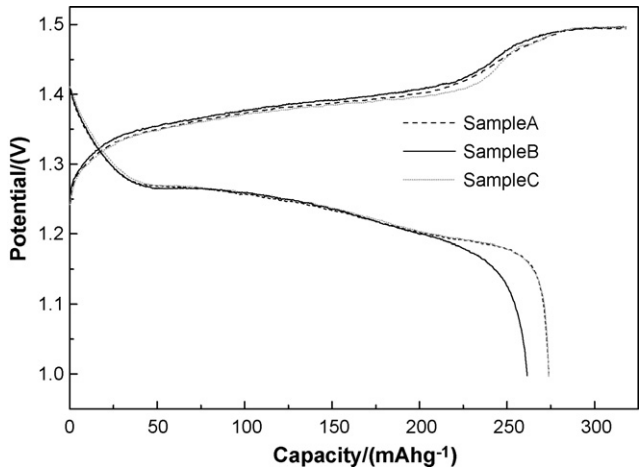

Fig. 12. Charge/discharge curves of samples A–C at 1*C* and 25 °C.

in Fig. 12. It can be seen that the charge and discharge curves of samples A and C are almost identical, whereas sample B presents a little lower discharge capacity.

The charge/discharge curves of the three samples at 60 °C are given in Fig. 13.The ratio of the discharge capacity of samples B and C at 60 °C over that at 25 °C can reach 77.6 and 88.1%, respectively. In contrast, the ratio for sample A is only 45.4%. Additionally, for samples B and C, a rise in charging potential at the end of charge indicates that the charging reaction of Ni(II) to Ni(III) and the side reactions proceed in series way. Sample A, by contrast, exhibits no such rise of the charging potential at the end of charge, which indicates that the main and side reactions occur in parallel way.

Above results have shown that the $Y(OH)_3$ coating is an effective way to improve charging acceptance of $Ni(OH)_2$ at elevated temperature, and the necessary coating amount is only 0.55 at.%, which is smaller than that of yttrium doping (1 at.%) [14], $Yb(OH)_3$ coating (2 at.%) [30], $Ca_3(PO)_4$ coating (2 at.%) [31] and $Lu(OH)_3$ coating (0.8 at.%) [32]. In recent reports [14,30–32], the majority of the researchers regarded the reason for the similar improvement as the contribution of the overvoltage increase for oxygen evolution reaction. Based on the CV

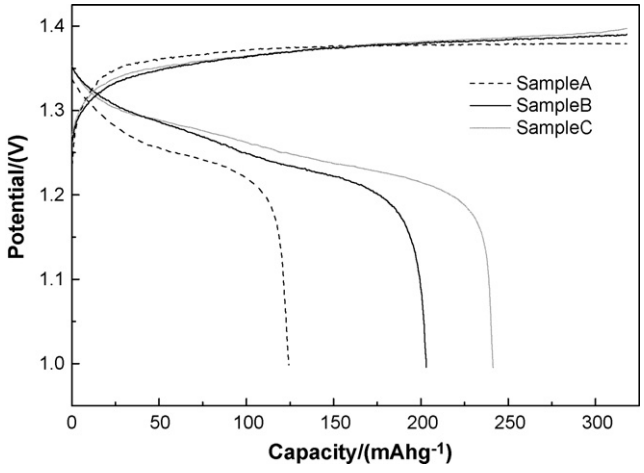

Fig. 13. Charge/discharge curves of samples A–C at 1*C* and 60 °C.

results in this study, the formation of unstable Ni(IV) species is considered as another side reaction. The conflict between Ni(II) and Ni(III) oxidation reactions exists in the charging process and becomes more drastic at elevated temperatures. The charge acceptance of $Ni(OH)_2$ electrode should be increased either by restraining the Ni(III) oxidation reaction or by making Ni(IV) species more stable. Obviously, the latter way is also beneficial to increasing the specific capacity of $Ni(OH)_2$ electrode. However, this deduction is disagreeable with our results that after $Y(OH)_3$ coating the electrode capacity decreased at 25 °C. Meanwhile, there is only one reduction current peak in CV measurements (see Fig. 4). On the other hand, both CV and charge/discharge test results have shown that the coating layer of $Y(OH)_3$ can effectively enhance the potential difference between the main and the side reactions at elevated temperatures. Therefore, the increase of the charge acceptance after $Y(OH)_3$ coating can be ascribed to the restraining function of it for both the oxygen evolution and the Ni(III) oxidation reactions.

From Fig. 13, it is also noted that sample C is more effective for improving the charge acceptance of $Ni(OH)_2$ electrode at elevated temperature. The results agree well with those of CV experiments. The interesting question is why the effects of surface coating of $Y(OH)_3$ are diverse for samples B and C, though the additive amounts of them are nearly the same. This may be explained as follows. From SEM images, it can be seen that the surface of sample B is smooth, dense and nonporous, whereas the surface of sample C is coarse and porous. The images imply that $Y(OH)_3$ precipitates of sample B are formed partially inside the pores between tiny crystals, but for sample C the majority of $Y(OH)_3$ are precipitated on the surface of $Ni(OH)_2$ crystals. From XPS analysis, it is found that the molar ratio of element Y to Ni on the surface of sample B is much less than that of sample C. The results indicate that in sample B some parts of the surface of $Ni(OH)_2$ crystals are still uncoated, while the distribution of yttrium on the surface of sample C is more uniform. The CV and charge/discharge tests have proved that sample C is more effective on suppressing the oxygen evolution reactions and the formation of Ni(IV) on the surface of spherical $Ni(OH)_2$. Therefore, we consider that the enriched yttrium on the surface of $Ni(OH)_2$ crystals is beneficial to controlling the side reactions, while $Y(OH)_3$ precipitated inside the pores between tiny crystals is less effective.

On the basis of these facts, it can be concluded that the improvement of the high-temperature performance of $Ni(OH)_2$ electrode is not only related to the effects of additives themselves, but also depends on the distribution of these adding elements in surface oxide layer of $Ni(OH)_2$. The coating surface with dense and porous morphology, larger relative surface content and higher utilization ratio of yttrium is more effective on suppressing the side reactions and improving the high-temperature performance of $Ni(OH)_2$ electrode.

4. Conclusions

The electrochemical oxidation/reduction properties of spherical β-$Ni(OH)_2$ with similar diameters were studied by

cyclic voltammetry with SE-E. This technique provided some unique information about a two-step oxidation process corresponding to the successive transitions: Ni(II) → Ni(III) and Ni(III) → Ni(IV). Following conclusions can be made:

(1) For spherical $Ni(OH)_2$, the Ni(IV) species formed in the charging process are not stable and can be totally converted into Ni(III) species accompanied by oxygen evolution. The conversion of Ni(III) to Ni(IV), which may take place on the surface layer of the particle, is regarded as a side reaction, and it can result in the decline of charge acceptance.
(2) Spherical $Ni(OH)_2$ was successfully modified with $Y(OH)_3$ by chemical surface precipitation. Two distinct samples with diverse morphologies were obtained under different experimental conditions.
(3) The presence of the coated $Y(OH)_3$ can restrain the side reactions including oxygen evolution and Ni(III) oxidation reactions, especially in the potential range close to Ni(II) oxidation reaction. The chemical nature and morphology of the coating layer play an important role in controlling the side reactions.
(4) The charge acceptance of the electrode with 0.55 at.% Y-coated $Ni(OH)_2$ reaches 88.1% at 60 °C. The high-temperature performance of $Ni(OH)_2$ electrode is related to the distribution of the adding elements in surface oxide layer of $Ni(OH)_2$. The coating surface with dense and porous morphology, larger relative surface content and higher utilization ratio of yttrium is more effective.

Acknowledgements

The financial support by the 863 National Research and Development Project Foundation of China (Grant No. 2005AA501440) is gratefully acknowledged.

References

[1] Y.J. Kim, S. Srinivasan, A.J. Appleby, J. Appl. Electrochem. 20 (1990) 377.
[2] K. Micha, Z. Zabransky, M. Svata, J. Power sources 8 (1982) 9.
[3] J. Chen, D.H. Bradhurst, S.X. Dou, H.K. Liu, J. Electrochem. Soc. 146 (1999) 3606.
[4] W.E. O'Grady, K.I. Pandya, K.E. Swider, D.A. Corrigan, J. Electrochem. Soc. 143 (1996) 1613.
[5] D.A. Corrigan, S.L. Knight, J. Electrochem. Soc. 136 (1989) 613.
[6] J. Desilvestro, D.A. Corrigan, M.J. Weaver, J. Electrochem. Soc. 135 (1988) 885.
[7] B.E. Conway, M.A. Sattar, J. Electroanal. Chem. 19 (1968) 351.
[8] P.W.T. Lu, S. Srinivasan, J. Electrochem. Soc. 125 (1978) 1416.
[9] L. Indira, M. Dixit, P.V. Kamath, J. Power sources 52 (1994) 93.
[10] R.D. Armstrong, E.A. Charles, J. Power sources 25 (1989) 89.
[11] Y.S. Zhang, X.Y. Cao, H.T. Yuan, W.H. Zhang, Z.X. Zhou, Int. J. Hydrogen Energy 24 (1999) 529.
[12] G.T. Cheek, W.E. O'Grady, J. Electroanal. Chem. 421 (1997) 173.
[13] Y. Morioka, S. Narukawa, T. Itou, J. Power sources 100 (2001) 107.
[14] X. Mi, X.P. Gao, C.Y. Jiang, M.M. Geng, J. Yan, C.R. Wan, Electrochim. Acta 49 (2004) 3361.
[15] F.Y. Cheng, J. Chen, P.W. Shen, J. Power Sources 150 (2005) 255.
[16] D. Singh, J. Electrochem. Soc. 145 (1998) 116.
[17] H. Bode, K. Dehmelt, J. Witte, Electrochim. Acta 11 (1966) 1079.
[18] H.B. Zhou, Z.T. Zhou, Solid State Ionics 176 (2005) 1909.
[19] M. Wohlfahrt-Mehrens, R. Oesten, P. Wilde, R.A. Huggins, Solid State Ionics 86–88 (1996) 841.
[20] I.G. Casella, M.R. Guascito, M.G. Sannazzaro, J. Electroanal. Chem. 462 (1999) 202.
[21] M. Paszkiewicz, I. Walas, Electrochim. Acta 24 (1979) 629.
[22] B. Liu, H.T. Yuan, Y.S. Zhang, Int. J. Hydrogen Energy 29 (2004) 453.
[23] X.Y. Wang, J. Yan, Y.S. Zhang, H.T. Yuan, D.Y. Song, J. Appl. Electrochem. 28 (1998) 1377.
[24] R.D. Armstrong, G.W.D. Briggs, E.A. Charles, J. Appl. Electrochem. 18 (1988) 215.
[25] W.K. Hu, X.P. Gao, D. Noreus, T. Burchardt, N.K. Nakstad, J. Power sources 160 (2006) 704.
[26] X.J. Han, X.M. Xie, C.Q. Xu, D.R. Zhou, Y.L. Ma, Opt. Mater. 23 (2003) 465.
[27] M. Oshitani, M. Watada, K. Shodai, M. Kodama, J. Electrochem. Soc. 148 (2001) A67.
[28] G. Bronoel, J. Reby, Electrochim. Acta 25 (1980) 973.
[29] W.K. Hu, X.P. Gao, M.M. Geng, Z.X. Gong, D. Noréus, J. Phys. Chem. B 109 (2005) 5392.
[30] X.M. He, L. Wang, W. Li, C.Y. Jiang, C.R. Wang, J. Power sources 158 (2006) 1480.
[31] X.M. He, J.G. Ren, W. Li, C.Y. Jiang, C.R. Wan, Electrochim. Acta 51 (2006) 4533.
[32] J.X. Ren, J. Yan, Z. Zhou, X.J. Wang, X.P. Gao, Int. J. Hydrogen Energy 31 (2006) 71.